Thermionic power generation at high temperatures using SiGe/Si superlattices

Daryoosh Vashaee[a] and Ali Shakouri
Jack Baskin School of Engineering, University of California, Santa Cruz, California 95064

(Received 11 July 2006; accepted 30 December 2006; published online 15 March 2007)

Recent studies have predicted that heterostructure superlattices can enhance the effective thermoelectric power factor significantly through selective emission of hot carriers via thermionic emission. Here, we study the potential of SiGe/Si superlattices for power generation at high temperatures. A detailed theory based on Boltzmann transport equation is developed which takes into account multiple valleys. We show that thermionic emission provides only a modest improvement in the power factor. This is due to the fact that SiGe is a multivalley semiconductor and it has a large density of states. With reasonable dopings, Fermi energy in SiGe alloy is very close to the band minimum so that the symmetry of the differential conductivity does not change very much with small barrier superlattices. Particularly at high temperatures when the thermal spread of the carriers is much larger than the Fermi energy in the band, superlattice energy filtering is not effective. © *2007 American Institute of Physics*. [DOI: 10.1063/1.2645607]

INTRODUCTION

Quite a few thermoelectric (TE) materials work well at high temperature. Examples are SiGe alloy, the group of filled skutterides,[1–3] and tellerium-antimony-gemanium-silver (TAG).[4–7] However, materials with improved thermoelectric properties are still needed to make power generators more efficient. It is known that SiGe is a much better TE material at higher temperature. Si–Ge alloys are also used in thermoelectric generators at high temperatures ($T \sim 1000$ K). The best known mixture is $Si_{0.7}Ge_{0.3}$. In this paper we will investigate the possibility of improving ZT of SiGe at high temperatures using thermionic emission in SiGe/Si superlattices. We will consider both n-type and p-type materials.

N-TYPE SiGe/Si SUPERLATTICE POWER GENERATOR

It is known that the minimum of the conduction band in silicon lies on the (100) direction inside the zone. Thus, there are effectively six equivalent conduction bands in silicon. In Ge the lowest conduction band minima are located at the L point of the zone. There are effectively four equivalent conduction bands in Ge. The isoenergetic surfaces are ellipsoids of revolution in both materials. For our purposes, we consider a $Si_{0.75}Ge_{0.25}$/Si superlattice with the parameters listed in Table I where n_w is the number of superlattice periods; L_w and L_b are the widths of well and barrier, respectively; V_b is the barrier height; $m^*_{X\text{-}w}$ and $m^*_{L\text{-}w}$ are the electron effective masses in the X and L valleys of the well region, respectively; $m^*_{X\text{-}b}$ and $m^*_{L\text{-}b}$ are the corresponding electron effective masses in the barrier region; β is the thermal conductivity; μ is the electron mobility; and $E_c(L)$ is the energy band minima at the L valley. For the calculation of the transport coefficients, we use the model presented in Ref. 10. In brief, a linear Boltzmann transport equation was used to calculate the thermoelectric characteristics of the SiGe bulk device. As for the superlattice properties, conventional bulk transport was modified by taking into account the effects of the two-dimensional states in the well and three-dimensional states both above the well and in the barrier regions. In addition, the quantum mechanical transmission coefficient for electron transport between wells was introduced in the Boltzmann equation. This takes into account both tunneling and thermionic emission. Since the barrier layer thickness is large enough for miniband transport to be negligible, the transmission probability is calculated using the Wentzel-Kramers-Brillouin (WKB) approximation. Finally, Fermi-Dirac statistics were used to account for the number of available empty states in the neighboring wells for tunneling and thermionic emission calculations. The L-valley transport has also been included in the electronic transport equations, as the minima of the energy band at the L valley are close to those of the band edge (~840 meV), which can be important in a highly degenerated structure. For this purpose, the electron transport is considered separately for each valley both in the well and barrier regions. The current densities were then added with a weighting factor based on the Fermi-Dirac distribution function.

The calculated effective thermoelectric properties of the SiGe alloy versus doping concentration are shown in Fig. 1. Two cases of electron transports in the superlattice are considered: when transverse momentum during thermionic emission is conserved and when transverse momentum is not conserved.[10–13] The plot shows that, in both cases, superlattice transport does not improve much the ZT over the bulk values.[14]

Basically, this is due to the small conduction band offset of the SiGe/Si superlattice, which is about 12% ($E_b \sim 23$ meV for the proposed structure). It is also seen that L-valley transport does not play a role at doping concentrations below 10^{20} cm^{-3}, where the maximum ZT happens. In

[a]Author to whom correspondence should be addressed; electronic mail: daryoosh@soe.ucsc.edu

TABLE I. Structure parameters for the *n*-type $Si_{0.75}Ge_{0.25}/Si$ superlattice.

n_w	L_w (nm)	L_b (nm)	V_b (meV)	$m^*_{X\text{-}w}$ (m_e)	$m^*_{L\text{-}w}$ (m_e)	$m^*_{X\text{-}b}$ (m_e)	$m^*_{L\text{-}b}$ (m_e)	β (W/mK)	μ ($cm^2/V\,s$)	$E_C(L)$ (meV)
50	30	10	22.8[a]	1	1.8	1.08	2	7.26–1.1[b]	61[c]	841[a]

[a]Reference 8.
[b]Values are calculated for $Si_{0.75}Ge_{0.25}$ alloy doped to 10^{16}–10^{21} cm^{-3}.
[c]Reference 9.

the next section, we will consider a *p*-type SiGe superlattice and calculate the corresponding thermoelectric properties.

P-TYPE SiGe/Si SUPERLATTICE POWER GENERATOR

A *p*-type SiGe based microcooler is considered and the thermoelectric properties of the superlattice and alloy are calculated. Electrothermal transport through both the light and heavy hole bands is taken into account. The model used in this section follows that of Ref. 10 as well. Parameters used in the simulation are listed in Table II. Mobility and thermal conductivity have been calculated as a function of carrier concentration and temperature.

Thermoelectric properties for the *p*-type SiGe bulk and superlattice versus doping concentration for four temperatures, $T=300$, 633, 966, and 1300 K, are calculated. Figure 2 shows the calculated electrical conductivity, Seebeck coefficient, Fermi energy, and thermoelectric figure of merit versus doping concentration for the SiGe alloy. A *ZT* of about 1 is estimated for the SiGe bulk at $T=1300$ K. Figure 3 shows the corresponding quantities for the *p*-type $Si_{0.75}Ge_{0.25}/Si$ superlattice, where we assume that the transverse momentum is conserved. In Fig. 4 the same quantities are calculated with the assumption that the transverse momentum is not conserved. In both cases, a ZT of about 1.2 is predicted. Comparing this to the *ZT* of 1 in the SiGe bulk material, we conclude that the thermionic filtering does not significantly improve the *ZT* of SiGe microcooler. This may seem counterintuitive. Materials with a higher asymmetry of differential conductivity $\sigma(E)$ have higher Seebeck coefficients. Larger effective mass causes more asymmetry in $\sigma(E)$. A hole's effective mass in *p*-type SiGe bulk is about $1.3m_e$, which results in a higher Seebeck coefficient than InGaAs and HgCdTe. Alternatively, a superlattice structure provides another way to increase the asymmetry of $\sigma(E)$. In fact, the effective Seebeck coefficient of a superlattice depends more directly on its structure than its carrier effective mass. Consequently, a superlattice can significantly increase the Seebeck coefficient of materials with smaller effective masses such as InGaAs or HgCdTe. However, the improvement in the Seebeck coefficient in a *p*-type SiGe superlattice is not significant compared to its bulk value as it is already high due to its large carrier effective mass (see Fig. 2–4). This can explain the reason that *ZT* of superlattice does not show a significant improvement compared to that of bulk material in the above simulations.

In order to gain better understanding, the differential conductivities of *p*-type bulk SiGe and those of the superlattice at different temperatures are plotted in Fig. 5. The same parameters as in Table II are used. Only the states below the barrier height are included in the calculations of the differential conductivity; moreover, the contribution of the states in the barrier region is ignored.[10]

The energy axis for the case where transverse momentum is conserved is the kinetic energy in the *z* direction, and for the case where transverse momentum is nonconserved, the energy axis is the total kinetic energy. It can be seen that at room temperature, a superlattice can increase the asymmetry of the differential conductivity. However, we have observed that at high temperatures, the electron distribution in the bulk is almost on one side of the Fermi level. This explains why we do not gain much improvement in *ZT* with a superlattice structure, as seen in Fig. 2–4. It is important to note that thermal conductivity is often reduced in superlattice structures. To emphasize the improvement in the thermoelectric figure of merit solely due to the thermionic emission of electrons over the barrier, the reduced thermal conductivity is not included in the above analysis.

It is also possible to explain why nonconservation of transverse momentum does not improve *ZT* at high temperatures. This matter is illustrated in Fig. 6. In this figure k_B is the Boltzmann constant, $E_b=\hbar^2k_b^2/2m$, and $E_f=\hbar^2k_f^2/2m$. It is also assumed that only states within $4k_BT$ of the Fermi energy (i.e., $k<k_f+\sqrt{8mk_BT/\hbar}$) can participate in transport. As the temperature increases, electron distribution around the Fermi level is broadened. Consequently, the number of states above the barrier ($k_z>k_b$) increases. These states participate in transport both in the case of conserved and nonconserved transverse momenta. While the volume of these states increases in three dimensions (k_x, k_y, and k_z) in *k* space, the volume of the states that participate in transport only when the transverse momentum is not conserved ($k>k_b$ and

TABLE II. Structure parameters for the *p*-type $Si_{0.75}Ge_{0.25}/Si$ superlattice.

n_w	L_w (nm)	L_b (nm)	V_b (meV)	m^*_{lh} (m_e)	m^*_{hh} (m_e)	β (W/mK)	μ ($cm^2/V\,s$)
50	30	10	167.4[a]	0.124	0.467	6.67–0.52[b]	155.9–32.8[b]

[a]Reference 8.
[b]Values are calculated for doping concentrations of 10^{16}–10^{21} cm^{-3} at $T=300$ K (Ref. 15).

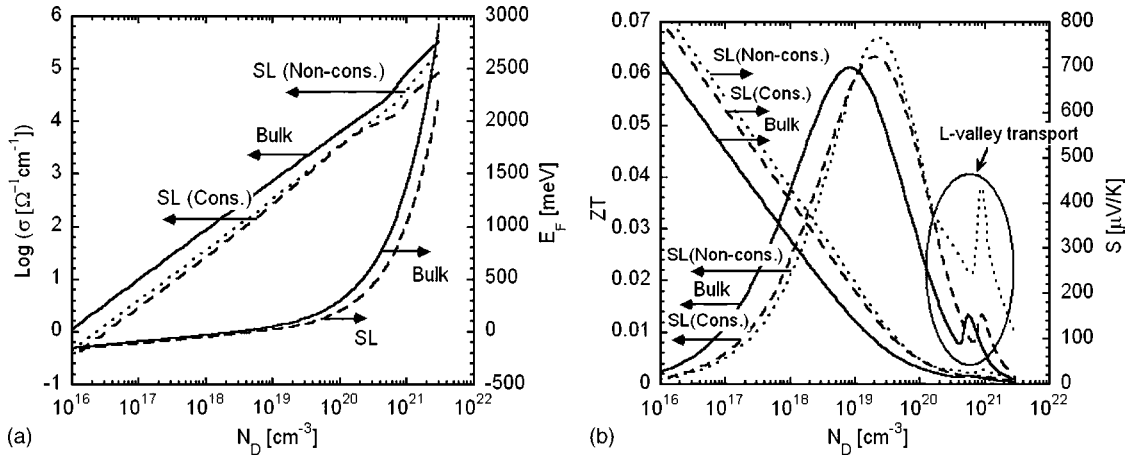

FIG. 1. Fermi energy (left-right axis), electrical conductivity (left-left axis), Seebeck coefficient (right-right axis), and thermoelectric figure of merit (right-left axis) of *n*-type $Si_{0.75}Ge_{0.25}$/Si superlattice vs doping concentration at $T=300$ K.

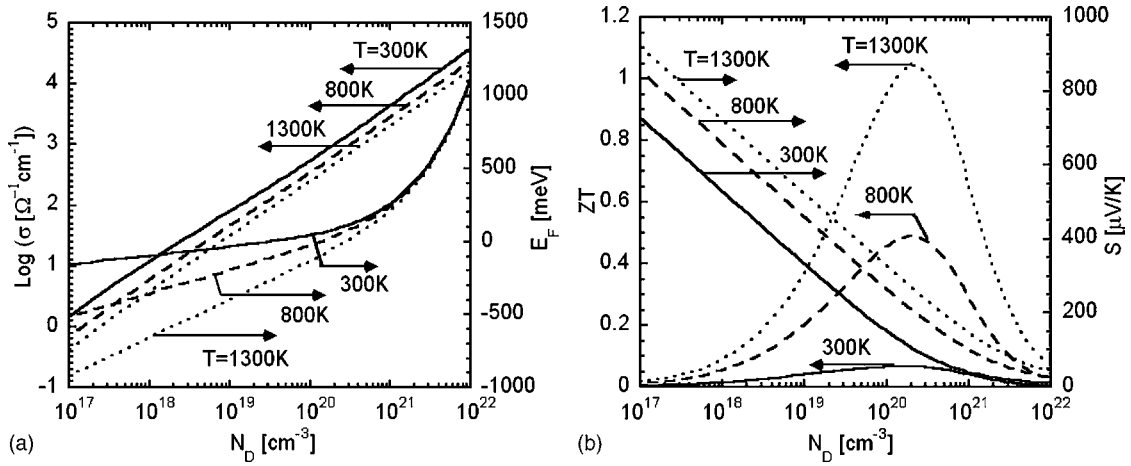

FIG. 2. Fermi energy (left-right axis), electrical conductivity (left-left axis), Seebeck coefficient (right-right axis), and thermoelectric figure of merit (right-left axis) of *p*-type $Si_{0.75}Ge_{0.25}$ bulk vs doping concentration at $T=300$, 633, 966, and 1300 K.

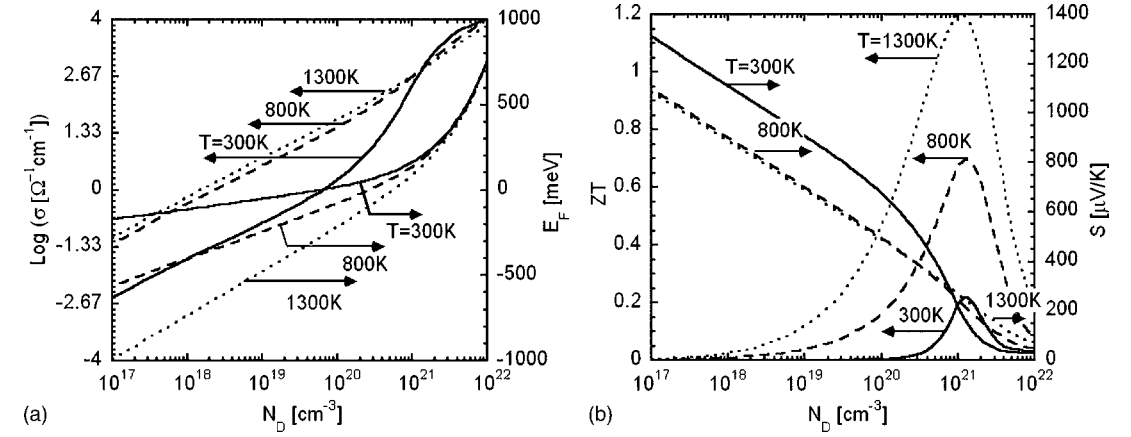

FIG. 3. Fermi energy (left-right axis), electrical conductivity (left-left axis), Seebeck coefficient (right-right axis), and thermoelectric figure of merit (right-left axis) of *p*-type $Si_{0.75}Ge_{0.25}$/Si superlattice vs doping concentration assuming that the transverse momentum is conserved at $T=300$, 633, 966, and 1300 K.

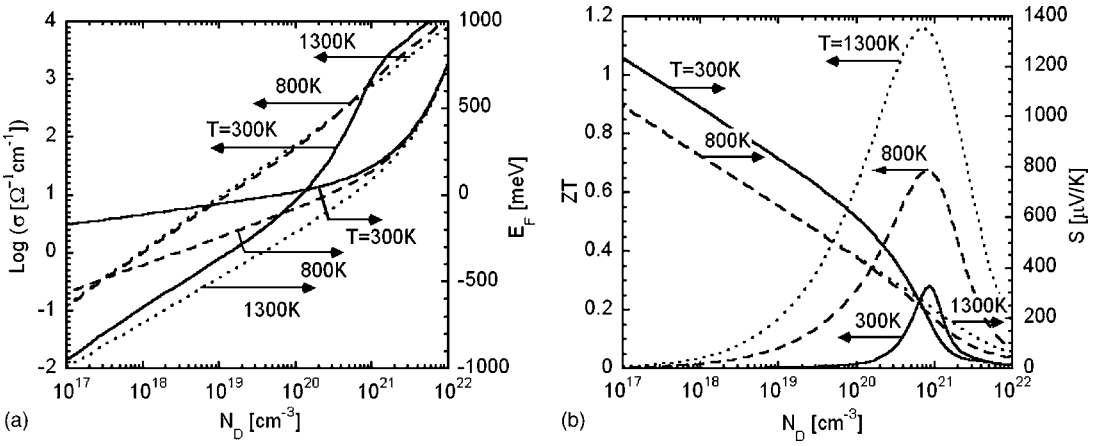

FIG. 4. Fermi energy (left-right axis), electrical conductivity (left-left axis), Seebeck coefficient (right-right axis), and thermoelectric figure of merit (right-left axis) of *p*-type $Si_{0.75}Ge_{0.25}/Si$ superlattice vs doping concentration assuming that the transverse momentum is not conserved at $T=300$, 633, 966, and 1300 K.

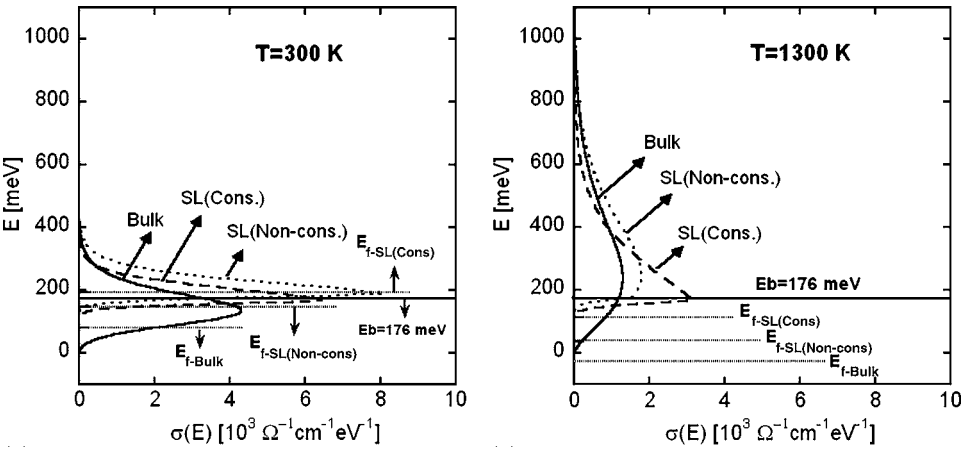

FIG. 5. Differential conductivity vs electron energy for the three cases of bulk SiGe (solid), SiGe superlattice assuming the transverse momentum is conserved (dashed) and is not conserved (dotted). Two temperatures of 300 K (left) and 1300 K (right) are considered. Barrier height and the optimum Fermi energy for each case are shown with horizontal lines on the plots.

$k_z < k_b$) increases in two dimensions (k_x and k_y). This results in the small effect of the lateral momentum conservation on high temperature electrical conductivity of the superlattice.

CONCLUSION

Heterostructure thermionic devices have shown a remarkable potential to improve the thermoelectric power factors at room temperature. The two key factors in the improvement of the thermoelectric power factor in these devices are the induced asymmetric differential conductivity by the potential barrier and nonconservation of transverse momentum in thermionic emission. The former factor results in a higher Seebeck coefficient and the latter one dramatically increases the number of electrons transmitted over the barrier. As these electrons are responsible for thermionic emission, thermionic power factor is increased. In this paper, we explored the effective thermoelectric properties of

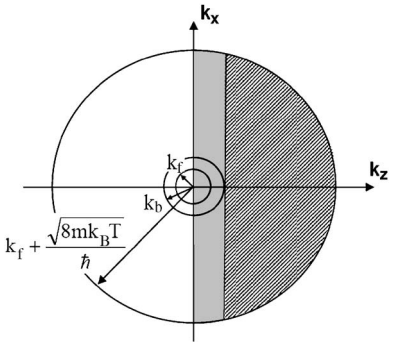

FIG. 6. Electronic states shown in k space. States with $k_z > k_b$ (patterned area) and $k < k_b$ (patterned plus gray filled area) participate in transport when the transverse momentum is or is not conserved, respectively. The ratio of the number of these states approaches unity as the temperature increases.

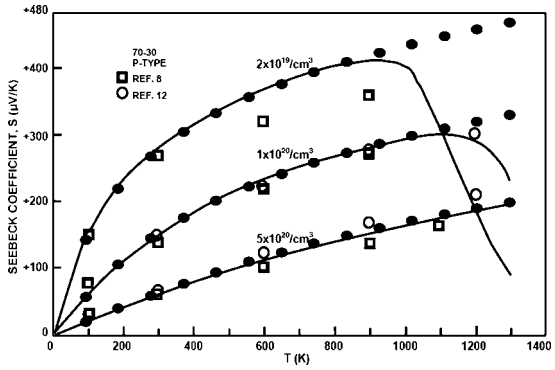

FIG. 7. Seebeck coefficient of *p*-type Si–Ge as a function of temperature calculated by Slack *et al.* (Ref. 15) The experimental points are from the literature (Refs. 16 and 17) The data from Abrikosov *et al.* (Ref. 16) are for the three compositions listed; the data from Dismukes *et al.* (Ref. 17) are for 0.89×10^{20} and 3.5×10^{20} cm^{-3}. Solid circles show our calculated Seebeck coefficients for the same structures.

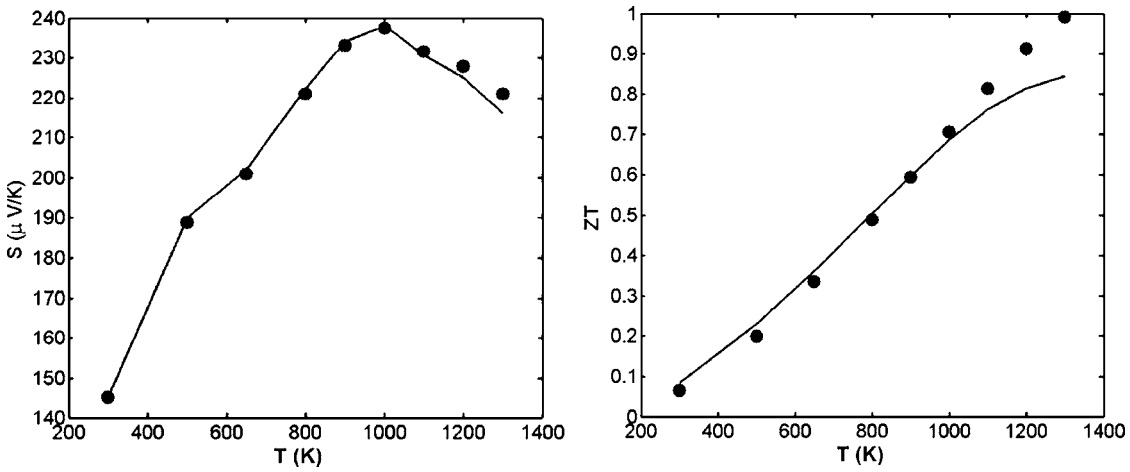

FIG. 8. Seebeck coefficient (left) and figure of merit (right) of *p* type SiGe as a function of temperature calculated in Ref. 15. Solid circles show the calculated Seebeck coefficient using our model.

SiGe/Si heterostructure superlattice for use in high temperature applications. We studied two limiting cases based on the conservation of transverse momentum to determine the number of electrons participating in the thermionic emission process. It is shown that the induced differential conductivity in SiGe/Si superlattices does not provide a significant improvement in the power factor at high temperatures. We also showed that the nonconservation of transverse momentum does not provide major improvement. These are consequences of large density of electronic states near the band edge and the requirement for small barrier superlattices for reasonable doping densities. As a result, a significant improvement in thermoelectric power factor in SiGe/Si heterostructure superlattices at high temperatures should mainly come from the reduced lattice thermal conductivity or other means to increase the thermoelectric power factor (a change in electron effective mass or mobility that could happen with, e.g., large amount of strain in the material).

APPENDIX: COMPARISON WITH EXPERIMENTAL DATA

In order to verify the model used in the simulations of the thermoelectric properties of the *p*-type SiGe microcoolers, three different data sets are considered and simulated. One data set is from Slack *et al.*[15] on the Seebeck coefficient of *p*-type SiGe single crystal alloy. Figure 7 shows the agreement between our model and the experimental data for the Seebeck coefficient of the samples given in Ref. 15. The agreement is very good.

As another example, the Seebeck coefficient and figure of merit (*ZT*) of SiGe cooler at different temperatures is calculated and compared with the model used in Ref. 15. Figure 8 shows the comparison of the calculated quantities. In this simulation, we have included the effects of temperature-dependent alloy scattering and carrier-phonon scattering in the calculation of the hole mobility in SiGe alloy following the model presented in Ref. 15. As for the calculation of thermal conductivity, we have included the temperature-dependent polar thermal conductivity in addition to lattice thermal conductivity. However, we have ignored the bipolar thermal conductivity, which is more important in a *n*-type SiGe alloy. The calculations were carried out at nine fixed temperatures of 300, 500, 650, 800, 900, 1000, 1100, 1200, and 1300 K over the dopant concentration range of 2×10^{19} 1×10^{21} cm^{-3} for *p*-type samples. The maximum *ZT* was chosen for the plots.

A good agreement between theory and experiment is obtained. The model for the superlattice transport we presented was verified with experimental data elsewhere,[10,18] so it is not discussed further here.

[1]B. C. Sales, D. Mandrus, and R. K. Williams, Science **272**, 1325 (1996).
[2]J. P. Fleurial *et al.*, Proceedings of the 15th International Conference on Thermoelectrics, Pasadena, CA, 26–29 March 1996 (unpublished).
[3]G. P. Meisner, Physica B & C **108B**, 763 (1981).
[4]F. D. Rosi, J. P. Dismukes, and E. F. Hockings, Electron. Eng. (U.K.) **79**, 450 (1960).
[5]S. K. Decheva-Plachkova, Phys. Status Solidi B **119**, K97 (1983).
[6]S. K. Plachkova, Phys. Status Solidi B **122**, L53 (1984).
[7]E. A. Skrabek and D. S. Trimmer, in *CRC Handbook of Thermoelectrics*, edited by D. M. Rowe (CRC, Boca Raton, FL, 1995), pp. 267–276.
[8]V. Palankovski, Ph.D. thesis, Technical University Vienna, 2000.
[9]As no data on the mobility of electrons in *L* valley were found, it is assumed equal to that of *X* valley.
[10]D. Vashaee and A. Shakouri, J. Appl. Phys. **95**, 1233 (2004).
[11]D. Vashaee and A. Shakouri, Phys. Rev. Lett. **92**, 106103 (2004).
[12]D. L. Smith *et al.*, Phys. Rev. Lett. **80**, 2433 (1998).
[13]D. Vashaee and A. Shakouri, Mater. Res. Soc. Symp. Proc. **691**, 131 (2001).
[14]Transport equations are written separately for the well and barrier regions. Thus, it is possible to use different mobilities for each region. As the barrier region is undoped, the carrier mobility is higher in that region than in the well region. On the other hand, the superlattice mobility is usually smaller than that of the bulk. Therefore, to avoid overestimation, the higher mobility of the barrier region (Si undoped) is not taken to be different from that of the doped region. An equal mobility is assumed everywhere as that of the well region (SiGe doped). This can be an underestimation for the calculated *ZT*; nevertheless, the effective *ZT* is not expected to be much improved through thermionic filtering, as the barrier height is very small.
[15]Slack *et al.*, J. Appl. Phys. **70**, 2694 (1991).
[16]N. Kh. Abrikosov, V. S. Zemskov, E. K. Iordanishvili, A. V. Petrov, and V. V. Rozhdestvenskaya, Fiz. Tekh. Poluprovodn. (S.-Peterburg) **2**, 1762 (1968) [Sov. Phys. Semicond. **2**, 1468 (1969)].
[17]J. P. Dismukes, L. Ekstrom, E. F. Steigmeier, I. Kudman, and D. S. Beers, J. Appl. Phys. **35**, 2899 (1964); B. Abeles and R. W. Cohen, *ibid.* **35**, 247 (1964).
[18]D. Vashaee *et al.* (unpublished).